DEU FMD 27(80) (2025) 189-198

Dokuz Eylül Üniversitesi Mühendislik Fakültesi Fen ve Mühendislik Dergisi
Dokuz Eylul University Faculty of Engineering Journal of Science and Engineering
Elektronik/Online ISSN: 2547-958X

RESEARCH ARTICLE / ARAŞTIRMA MAKALESI

Comprehensive Design of Slotless Permanent Magnet Synchronous Motors: Effects of Series and Parallel Turns

Oluksuz Sürekli Mıknatıslı Senkron Motorların Kapsamlı Tasarımı: Seri ve Paralel Sarım Sayılarının Etkisi

Yusuf Basri Yılmaz *, **Emine Bostancı**

Orta Doğu Teknik Üniversitesi Elektrik-Elektronik Mühendisliği Bölümü, Ankara, TÜRKİYE
*Corresponding Author / Sorumlu Yazar **: ybyilmaz@metu.edu.tr

Abstract

A comprehensive design methodology of a slotless permanent magnet synchronous machine (PMSM) based on a grid search and elimination method is presented in this study. The design process aims to investigate the effects of various design choices on machine cost and efficiency but not to obtain an optimal design. A high precision long cylinder type actuator with 1 kW rated power, 12,000 rpm rated speed, 50 mm diameter, and 135 mm maximum axial length is selected as the target design. The performance of design candidates is evaluated using an analytical model that includes the calculation of magnetic flux density, induced voltage, torque, and phase conductor losses. As the phase conductors are directly exposed to air-gap flux, conductor losses are calculated considering the the air-gap magnetic field. Due to this effect, the conductor design in slotless PMSMs should be done carefully. Therefore, in the next step, first the designs that satisfy the application requirements are distinguished, and then the series turn numbers as well as wire diameters and parallel turn numbers are assigned to each of them. Those assignments are made based on assumptions that assure the manufacturability of the winding. All the output designs are depicted with respect to their magnet volume and winding conductor losses to obtain a Pareto-optimal front curve. Thus, the effects of different design decisions on these two performance variables were observed. As expected, the designs with a high number of parallel turns have higher efficiencies. Furthermore, when the designs with the same number of parallel turns are compared, the ones with smaller permanent magnet volumes are found to be preferable since the total cost of their raw materials is around 20% cheaper with almost no difference in their efficiencies.

Keywords: *Slotless machine, permanent magnet synchronous machine, analytical magnetic field calculation, hexagonal winding, turn number*

Öz

Oluksuz sürekli mıknatıslı bir senkron motorun ızgara araması ve eleme yöntemine dayanarak yapılmış kapsamlı tasarım metodolojisi bu çalışmada sunulmaktadır. Tasarım sürecinin amacı, çeşitli tasarım seçeneklerinin motor maliyeti ve verimliliği üzerindeki etkilerini araştırmak, ancak optimal bir tasarım elde etmek değildir. Hedef tasarım olarak, 1 kW nominal güç, 12,000 devir/dakika nominal hız, 50 mm çapında ve 135 mm maksimum eksenel uzunluğa sahip yüksek hassasiyetli uzun silindir tipi bir aktüatör seçilmiştir. Tasarım adaylarının performansı, manyetik akı yoğunluğu, indüklenen gerilim, moment ve faz iletkeni kayıplarının hesaplanmasını içeren analitik bir model kullanılarak değerlendirilir. Faz iletkenleri doğrudan hava aralığı akısına maruz kaldığından, iletken kayıpları hava aralığı manyetik alan dikkate alınarak hesaplanır. Bu etkiden dolayı oluksuz PMSM'lerdeki iletken tasarımı dikkatli yapılmalıdır. Bu nedenle bir sonraki adımda öncelikle uygulama gereksinimlerini karşılayan tasarımlar ayrıştırılmakta ve sonrasında her birine olası seri sarım sayıları ile tel çapları ve paralel sarım sayıları atanmaktadır. Bu atamalar, sarımın üretilebilirliğini garanti eden varsayımlara dayalı olarak yapılır. Pareto-optimal bir ön eğri elde etmek için tüm çıkış tasarımları mıknatıs hacimlerine ve sargı iletken kayıplarına göre tasvir edilmiştir. Böylelikle farklı tasarım kararlarının bu iki performans kriterine etkileri gözlemlenmiştir. Beklendiği üzere, paralel sarım sayısı fazla olan tasarımların verimliliği daha yüksek bulunmuştur. Ayrıca aynı sayıda paralel sarımlı tasarımlar karşılaştırıldığında, kalıcı mıknatıs hacimleri daha küçük olanların, hammaddelerinin toplam maliyetinin %20 civarında daha ucuz olması ve verimliliklerinde de neredeyse hiç fark olmaması nedeniyle daha avantajlı oldukları görülmektedir.

Anahtar Kelimeler: *Oluksuz makina, kalıcı mıknatıslı senkron makina, analitik manyetik akı hesabı, altıgen şeklinde sarım, sarım tur sayısı*

1. Introduction

Slotless permanent magnet synchronous machines (PMSMs) and slotless brushless DC (BLDC) machines have a round stator core with no slots and mostly surface mount or surface inset PM rotors. These machines are also known as slotless permanent magnet (PM) machines. It is a common practice to design coils with no winding overhang to increase the power density and also ease the cooling of the winding conductors. Based on their rotor and stator structures, slotless PM machines have a large effective air-gap, and hence lower torque densities as well as high copper losses compared to their slotted counterparts [1]. On the other hand, they have almost negligible torque ripple, a linear operational characteristic and low core losses. Their torque outputs have no cogging torque as it originates from the interaction between slots and permanent magnets and slotless machines do not have slotting effect. So, they are a good option for high-precision applications such as surgery arms and

DOI: https://doi.org/10.21205/deufmd.2025278004

Geliş Tarihi / Received: 28.12.2023
Kabul Tarihi / Accepted: 30.07.2024

aerospace applications. Moreover, a slotless topology is one of the few options to achieve a relatively high power density and a very low torque ripple with a limited radial dimension. These features make them suitable for high precision, high power density and high speed applications.

Analytical calculation methods are generally used in the design and analysis of slotless PM machines due to their simple magnetic structures. Whereas, finite element analysis (FEA) is relatively uncommon due to 3-D nature of the most slotless machines but used to verify the analytical results. There are various studies on the calculation of machine characteristics such as torque output, back-EMF and losses based on analytical magnetic field expressions as in [2]. Different magnetic patterns such as radially magnetized, diametrically magnetized and Halbach-array PMs are considered in these studies.

Besides, there are several studies focusing on optimization of slotless PM machines. Chen et al [7] uses analytical and FEA results to determine the optimal PM and winding area thicknesses as rotor and stator dimensions, pole numbers, PM magnetization patterns and pole arc vary for a single layer rectangular winding design. In [8], a design methodology, where the analytical expressions for torque, power and losses are used, is presented. Radial distance between PMs and rotor back iron field density are identified as free parameters and the other machine parameters are determined based on the specifications. As an exemplary result, minimum mass of the machine as efficiency criterion changes is presented. Design optimization aiming minimum losses for selected machine dimensions is studied in [9] for a 2 kW 200 krpm machine. Winding resistive losses and core losses are estimated analytically, and main attention is given to mechanical losses due to very high speed of the application. In [10], an improved particle swarm optimization is presented and compared with conventional algorithms for 3 different stator phase current waveforms. The objective function is selected to minimize the total losses, which include winding resistive losses, core losses and PM eddy current losses, and machine volume for a given torque, speed and stator-core magnetic flux density by using analytical expressions. In all these studies mentioned above, either a single layer rectangular winding structure is assumed or no information on winding type is included.

Moreover, eddy current losses on phase conductors due to external PM field and effects of number of parallel turns are not considered. Eddy current losses in the windings due to external PM field are calculated in [11] by using coefficients that obtained by Ferreira method, however, number of parallel connections is not considered. Recently in [12], such losses are called open-circuit AC winding loss and effects of number of parallel turns are considered. Analytical field calculation method is adopted for minimizing the losses and number of parallel coils are maximized to minimize the open-circuit AC winding (eddy current losses due to external PM field). In our study, we put emphasize on the requirements of the coil structure to assure the manufacturability and assign multiple series and parallel number of turn numbers to each design to show the trade-offs.

The phase conductors of slotless PM machines are directly placed into the space between permanent magnets (PMs) and stator core. Thus, their coil structure is not constrained by slots and there are several options for optimization of the shape and placement of coils. Seo et al. [13] uses 2-D FEA results with corrections factors to account for the 3-D geometry due to hexagonal winding structure. For given rotor and stator radial dimensions, axial length of the machine as well as straight length and top angle of the winding are calculated to obtain the required torque output. The authors of [14] followed a different winding optimization method by trying to fit phase conductors into a given space to improve a machine constant defined as flux linkage area per square root of phase resistance. For that purpose, the hexagonal winding is divided into three sections and the axially straight length of the winding conductors are optimized. As winding shape approaches to a rectangular winding, the flux area increases but the available volume for the end winding conductors decreases so the conductor thickness. Therefore, there is an optimal axial straight length that is sought in that study and the main focus is the sizing of a given winding but not determining the number of series and parallel turns. Moreover, eddy current losses due to PM field are mentioned but not considered and given as a further study.

The existing design and optimization studies focus on specific aspects such as calculation of machine characteristics, winding optimization or comparisons between different magnetic structures [15]. However, an overall design procedure including the effects of the sizing of the machine parts along with the series and parallel turn numbers of winding on the machine characteristics is missing. Therefore, this study aims to present an overall design procedure for slotless PMSMs with the help of analytical and numerical calculations. The design process is developed for a machine to be used as an actuator with a speed of 12,000 rpm, therefore main attention is given to the cost and total copper loss minimization considering both the resistive and eddy current losses due to external PM field. An optimized solution is not sought, but pros and cons of different designs are investigated.

Analytical expressions for magnetic flux density distribution in the air-gap is studied in Section 2.1. Different winding structures are compared and an appropriate structure is chosen according to the application specifications in Section 2.2. The overall design procedure that is based on the grid search and elimination approach is explained in detail in Section 2.3. One of the output designs is taken as a reference and analytical results are validated with the help of 2-D and 3-D FEA simulations in Section 4. Finally, nine non-dominated design candidates that are chosen considering their raw material costs and phase conductor losses are compared in Section 5.

2. Material and Method

2.1. Analytical calculation of air-gap flux density

The air gap flux density of a slotless PM machine is mainly due to the PM flux as a result of a relatively large effective air gap [9]. Therefore, no-load (open-circuit) air-gap flux density distribution can be used to estimate machine performance. In this section, step by step derivation of the analytical expressions for no-load air-gap flux density distribution with diametrically magnetized PMs is given [3].

A basic PM slotless machine structure, including a shaft, PMs, and a stator, is shown in Figure 1. Phase conductors that are placed in the air gap are omitted since only the no-load flux density calculations are performed. The magnetic shaft and stator materials are assumed to have infinite permeability.

The starting point of the analytical calculations is the general relationship between magnetic field density B and magnetic field strength H. This relationship for air gap and PM material are given in (1), where the subscript m denotes PM material, μ_0 is the relative permeability of vacuum, and μ_r is the relative permeability and M is the magnetization of the PM material.

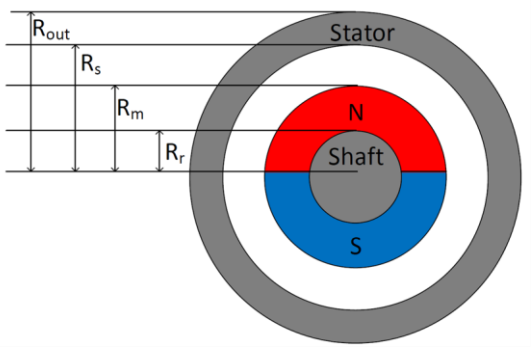

Figure 1. Cross section of slotless PM machine.

$$B_{air} = \mu_0 H_{air}$$
$$B_m = \mu_0(\mu_r H_m + M) \quad (1)$$

Fourier series method is used. The magnetization of PMs M is considered as a sum of the Fourier components. Since a diametrically magnetized PM is used, the magnetization composes of only the fundamental harmonics of the radial and tangential components as given in (2), where p is the pole pair number and θ is the angular rotor position.

$$M = Mcos(p\theta)\hat{a}_r + Msin(p\theta)\hat{a}_\theta \quad (2)$$

The radial and tangential flux density components in the air gap and in the PMs also include only the fundamental harmonics. Hence, the air-gap flux density of a slotless PMSM with diametrically magnetized PMs has a pure sinusoidal distribution. According to (1), H is needed for calculating the magnetic field density. As can be seen in (3), the gradient of the scalar magnetic potential φ can be used to calculate H.

$$H = -\nabla\varphi \quad (3)$$

Scalar magnetic potential obeys to Laplace's law, that is in the free space, Poisson's equation of the scalar magnetic potential is equal to zero as below.

$$\nabla^2\varphi_{air} = 0 \quad (4)$$

In the PM material, even if it is related to the divergence of the magnetic vector potential as in (5), it is also zero for the considered case since the divergence of the magnetization vector for a diametrically magnetized PM is zero.

$$\nabla^2\varphi_M = \frac{\nabla M}{\mu_r} \quad (5)$$

As a result, (4) and (5) can be expressed in the cylindrical coordinate system as follows:

$$\frac{\delta^2\varphi}{\delta r^2} + \frac{1}{r}\frac{\delta\varphi}{\delta r} + \frac{1}{r^2}\frac{\delta^2\varphi}{\delta\theta^2} = 0 \quad (6)$$

By using (6), the general solution of the scalar magnetic potential in the air gap and PM volumes can be expressed as in (7). A_{n1}, A_{n2}, B_{n1}, and B_{n2} are the coefficients of the homogeneous solution of the scalar magnetic potential, and they are different for the air gap and the PMs due to the boundary conditions. In this study, the machine is designed with one pole pair; thus, p in the following equations can be replaced by 1.

$$\varphi_{air} = (A_{n1}r^p + B_{n1}r^{-p})\cos(p\theta)$$
$$\varphi_m = (A_{n2}r^p + B_{n2}r^{-p})\cos(p\theta) \quad (7)$$

After the expressions in (7) are solved by considering the boundary conditions given in [2], the radial magnetic flux density is found as a function of the radius r and the angular displacement Θ as in (8), where Θ_m is the rotor position. R_r, R_m, R_s, and R_{out} are the radius of the machine parts as defined in Figure 1.

$$B_{air} = B_e\left(1 + \frac{R_s^2}{r^2}\right)\cos(\theta - \theta_m) \quad (8)$$

where B_e is defined as follows [8]:

$$B_e = \frac{B_r R_m^2(R_m^2 - R_r^2)}{(\mu_r + 1)R_m^2(R_s^2 - R_r^2) + (\mu_r - 1)(R_s^2 R_r^2 - R_m^4)} \quad (9)$$

The obtained B-field equation gives the air-gap magnetic flux density distribution in the r-Θ plane. The magnetic flux density distribution in the PMs can be obtained with a similar approach, but it is not investigated further since only the air-gap flux density distribution is used in the design process.

2.2. Winding structure

The most common winding types of a slotless PM machine [13] that are rectangular, rhombic, and hexagonal structures are shown in Figure 2.

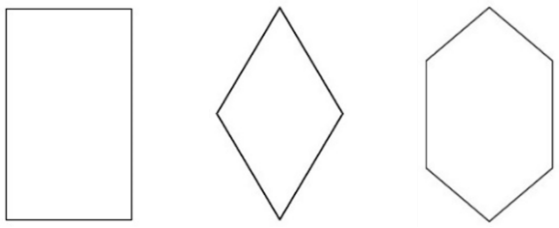

a. Rectangular **b**. Rhombic **c**. Hexagonal

Figure 2. Common winding structures.

The rectangular winding type has the highest flux linkage and induced voltage. However, its manufacturing is troublesome since the wires must be bend with 90° deg, and the space for interchanging the winding conductors is limited. In the rhombic winding, end winding connections are not a concern, but the flux linkage and the induced voltage are lower due to the decrease in the winding area. The hexagonal winding is a combination of the rectangular and the rhombic winding types.

In this study, the hexagonal winding type is selected since the target design has a long cylinder shape that is its diameter (50 mm) is relatively shorter than its axial length (135 mm). Moreover, double-layered concentric coils are assumed to be able to achieve a high fill factor. The span angle of each winding side is assumed to be 45° deg as shown in Figure 3-a. This means that there is a 135° deg angle difference between the innermost conductors of a winding that is represented by β_0, and there is a 15° deg empty space between the consequent phase conductors. These assumptions are made to guarantee a manufacturable winding. An exemplary winding is shown in Figure 3-c. Span angle of the n^{th} turn β_n of N total number of turns can be expressed as:

$$\beta_n = \beta_0 + \frac{45}{N}(2n-1) \quad (10)$$

The resultant fill factor is calculated by considering the span angle and the chosen wire structure. If the span angle were chosen to be 60° deg, it would not affect the fill factor. However, when it is chosen as 45° deg, it reduces the fill factor by 0.75. Moreover, round wires are used in this design, and fill factor due to wire geometry is assumed to be 0.5. The resultant fill factor is taken as 0.375, which is very close to the value used in other studies such as [8].

The top angle of the coils α is set to 120° deg as shown in Figure 3-b as a further design specification. This assures a fixed bend angle of the wire at all bending locations and minimizes any deformation of the wire insulation during bending. Based on this assumption, the axial length of the straight part of the conductors $L_{straight}$ can be determined by using the following expression.

$$L_{straight} = L_z - \frac{\beta_N R_c}{\tan(\alpha)} \quad (11)$$

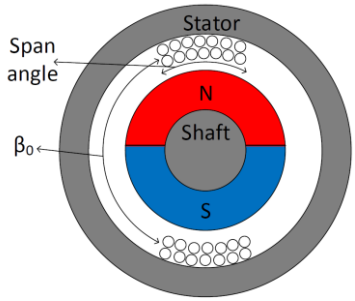

a. Cross section of a phase winding

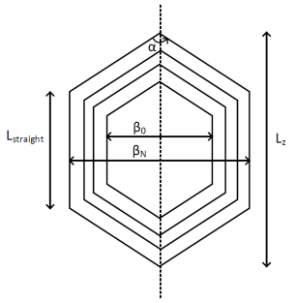

b. Hexagonal structure winding

c. Exemplary winding of a produced

Figure 3. Selected winding structure.

where L_z is the axial machine length, and R_c is the radial distance between the center of wires in the inner layer and the center of rotation. If the straight lengths of the turns are fixed, the top angle of each turn should be slightly different. However, this change is small for a machine with low aspect ratio and ignored in this step. The top angle of the outermost turn is taken as 120° deg, and it is assumed that others have the same top angle. A detailed winding placement and its manufacturing as in [14] is out of the scope of this study. It is rather focused on a winding design that can be conventionally winded.

2.3. Grid search based design process

After the flux density distribution in the air gap is calculated analytically and the general winding structure of the design is chosen, different design candidates can be evaluated. The flow chart of the design process is shown in Figure 4. As the first step, geometrical dimension limits, winding specifications, material characteristics and machine ratings given in Table 1 are set.

Table 1. Design spesifications and material characteristics.

Parameter	Value
Shaft radius (mm)	5
Outer radius (mm)	25
Axial length (mm)	135
Air gap* (mm)	0.5
Minimum magnet radius (mm)	9
Maximum magnet radius (mm)	14
Minimum inner stator yoke radius (mm)	12
Maximum inner stator yoke radius (mm)	20
Power (kW)	1
Operating speed (rpm)	12000
Operatin torque (Nm)	0.8
Resultant fill factor (slot)	0.375
Maximum current density (A/mm2)	5
Span angle of a coil side	45
Remanent flux density of PM (T)	1.19
Re-coil permeability of PM	1.09
Maximum stator flux density (T)	1.7
Drive voltage (VDC)	48

*Distance between PM surface and coils' inner radius

As the second step, the PM radius R_m and the stator inner radius R_s are varied between the maximum and minimum values given in Table 1 with 0.1 mm steps for $R_s > R_m$ + air gap. This gives the all possible design configurations. Then, the peak values of the flux density in the middle of the air-gap of all generated designs are calculated by using (8). In the rest of the design process, the designs that are not suitable are eliminated considering different design requirements.

The first design elimination is done considering the maximum flux density in the stator yoke. The maximum value of the yoke's flux density $B_{yoke-max}$ is calculated by assuming a homogeneous flux density distribution by using (12), where $B_{peak,r}$ is the peak value of the magnetic flux density on a radius r in the air-gap. In this process, the magnetic field due to the phase currents is ignored since the phase inductance L_{phase} of slotless machines is very small, so the corresponding field is negligible when compared to the PM field. Only the designs having a flux density lower than the saturation limit of the selected core material are kept for further consideration.

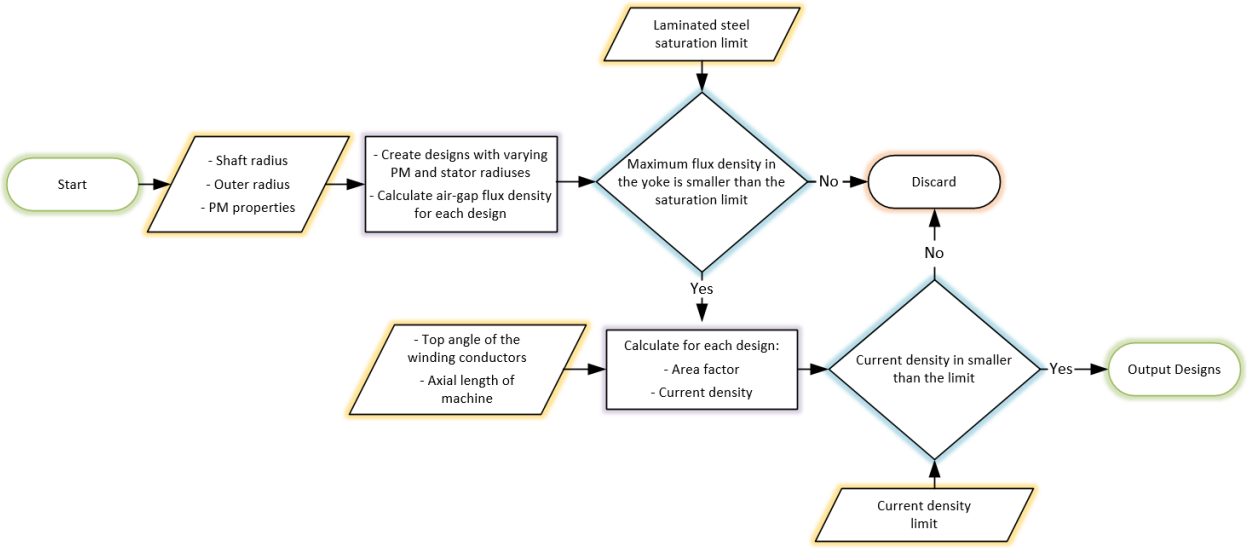

Figure 4. Design steps.

This is important since a higher flux density in the yoke causes saturation.

$$B_{yoke-max} = \frac{1}{R_{out} - R_s} \int_0^{\Pi} B_{peak,r} \sin(\theta)\, r d\theta \tag{12}$$

In the next step, the required current densities of the designs to accomplish the torque output specification are calculated. Generated torque can be calculated by using (13), where Ψ_{PM} is the flux linkage due to PM and i_q is the quadrature axis current. Since the number of series turns N is not determined yet, the Ni_q values to get the required torque can be found by writing the flux linkage of a phase as a function of N as in (14). The k_h correction factor in this equation is included to account for the decrease in the winding area due to hexagonal structure. The reduction in the flux linkage affects the torque production capability, thus the required Ni_q is inversely proportional to k_h.

$$T = \frac{3}{2} \Psi_{PM} i_q \tag{13}$$

where,

$$\Psi_{PM} = \frac{4}{\pi} L_z N B_e \frac{4R_s^3 - 3R_s^2 R_c - R_c^3}{R_s^2 - R_c^2} k_h$$
$$k_h = \frac{L_z + L_{straight}}{2L_z} \tag{14}$$

Eventually, the required current density can be calculated by using (15), where k_{fill} is the fill factor and A_{coil} is the coil area.

$$J = \frac{Ni_q}{A_{coil} k_{fill}}$$
$$A_{coil} = \frac{\pi(R_s^2 - (R_m + g)^2)}{6} \tag{15}$$

By using the imposed current density limitation, the designs whose current densities are higher than the limitation are eliminated. After all these eliminations are performed, the designs that fulfill the specifications are obtained.

2.4. Number of series and parallel turns

To conclude the design process, first the number of series turns and then the number of parallel turns of the phase conductors are assigned to each output design.

The iterative method shown in Figure 5 is used to find a proper series turn number N value for each output design. As can be seen, N is varied, and the resultant phase voltage at the rated speed is calculated. First, induced back EMF values at rated speed are determined. The no-load magnetic flux passing through nth turn ϕ_n is calculated. Here, the physical location of the turns is important. Therefore, the diameter of the conductors $D_{conductor}$ is updated as the turn number increases by using (16). Then, flux linkage is calculated by summing all ϕ_n values and it is differentiated with respect to time to get the induced back EMF as in (17).

$$D_{conductor} = \frac{\pi}{4} \frac{R_c}{N} \tag{16}$$

$$E_{ind} = \sum_{n=1}^{N} \frac{\delta \phi_n}{\delta t} \tag{17}$$

Moreover, the voltage drop on the phase inductance V_L is needed for terminal voltage calculation. The phase inductance L_{phase} can be estimated by using (18), where g^* is the effective air-gap length, including the PM, air gap and coil radial lengths. It is found that the voltage drops on the inductance of designs are in the 50 mV range at the operating frequency and current, and therefore their effect is ignored. After each iteration, the induced voltage is compared to the allowed phase voltage as in (19), and when it is higher than the phase voltage, iteration process is stopped, and the previous N value is taken. Allowed phase voltage is determined by considering DC-link voltage and the chosen PWM methodology which is SV-PWM. After N is assigned, i_q of the specific design can be found from its Ni_q value.

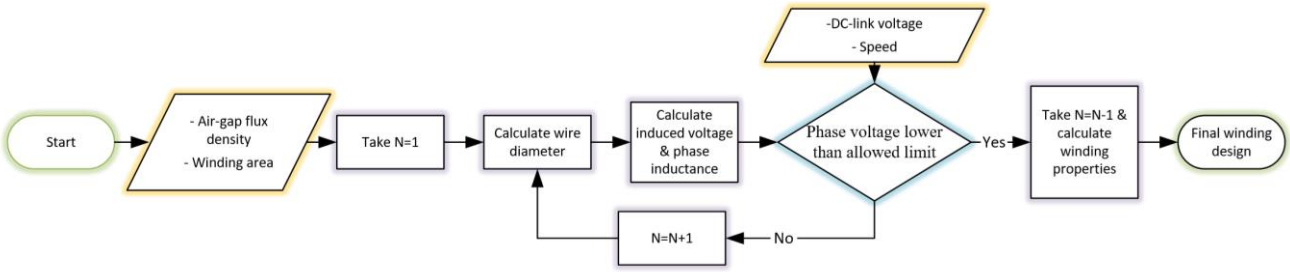

Figure 5. Determination of number of series turns for space vector pulse width modulation (SV-PWM) driven system.

$$L_{phase} = \frac{\pi}{4}\mu_0 N^2 \frac{R_c L_z}{g^*} \tag{18}$$

$$\frac{V_{dc}}{\sqrt{3}} \leq \sqrt{E_{ind}^2 + \left(\omega_e L_{phase} i_q\right)^2} \sim E_{ind} \tag{19}$$

The final winding design step is the determination of the wire diameter and the parallel turn number. The wire diameter must be carefully selected in PM slotless machines since the conductors are exposed to the PM field. This means, both the skin effect and the eddy currents induced due to the external PM field must be considered. The skin depth can be calculated by using (20), where ρ is the resistivity of the conductor, and f is the electrical frequency. The maximum electrical frequency of the machine is 200 Hz, and the corresponding skin depth is found as 4.61 mm for copper. However, much smaller wire diameters than this skin depth are selected to be able to fit N number of series turns in the air-gap and also to assure an easy wire bending process. Thus, the largest wire diameter is chosen as 1.291 mm, and the skin effect is neglected. In total, seven wire diameters that can be assigned to the output designs are predetermined: 0.723 mm, 0.812 mm, 0.912 mm, 1.024 mm, 1.15 mm, and 1.291 mm. The wires that give a fill factor that is enough to achieve the torque requirement within the current density limitation are assigned to each design. That means, if a design can be realized with different wires, all possible wire diameters are assigned to it to generate multiple candidate designs. It should be also mentioned that the geometrical limitations of the available winding area are taken into consideration during this process.

$$\delta = \sqrt{\frac{\rho}{\pi f \mu}} \tag{20}$$

So far, the designs that can produce the required torque within the design limitations are selected, and their turn numbers and wire dimensions are assigned. As the next step, the best design candidates should be selected. At this point, the cost and efficiency of the system are considered as the most important decision criteria. Accordingly, PM volume minimization is taken as the first selection criterion since it is directly related to the cost. Minimization of copper losses is selected as the second criterion since the dominant loss component of PM slotless machines at relatively low speed operations are the copper losses [1]. Core losses of the designs are expected to be in the same range, thus cannot be used as a distinguishing factor.

2.5. Analytical calculation of phase conductor losses

As discussed earlier, there will be two different copper loss mechanisms: the resistive losses due to the current flowing in the wire and the eddy current losses due to the external PM field on the wire [11]. Since each designs' wire properties such as diameter, length, and series and parallel turn numbers are available, the phase resistances are calculated and used to calculate the resistive copper losses of each design. The increase in resistance due to skin effect is ignored as wires with much smaller radiuses than the skin depth is chosen.

The second conductor loss component is calculated analytically with the help of the volumetric eddy current loss density equation for a long and thin rectangular conductor given in (21), where d is the thickness of the wire, ω is the electrical speed of the machine in rad/sec and σ is the conductivity of the conductor [20]. Since round wires are used in our designs, integration limits should be arranged for the cylindrical area. When this is done, the eddy current loss density per axial length for a round wire with a radius of r_c is obtained as given in (22).

$$p_{eddy-PM-rect} = \frac{2}{d}\int_0^{\frac{d}{2}} \frac{(x\omega\sigma B)^2}{2\sigma}\delta x \tag{21}$$

$$p_{eddy-PM-round} = 0.388\, B^2\omega^2\sigma r_c^4 \tag{22}$$

Equation (21) gives result in W/m^3 while (22) gives result in W/m. The total copper losses including the resistive losses and eddy current losses due to external magnetic field are calculated for each candidate design.

3. Results

3.1. Results of design procedure

Some of the valid design candidates are depicted in Figure 6 according to their PM volumes and total copper losses. Marker colors denote designs with different parallel turn numbers. Due to low phase inductance values, any voltage difference between parallel turns may cause high circulating currents. Therefore, parallel turn numbers higher than six are avoided to limit the circulating currents within a phase winding.

The designs with low PM volume should have a higher amount of copper, and a higher number of series turns to be able to meet the specifications. Therefore, it is expected to see an increase in the resistive copper losses as magnet volume decreases. On the other hand, as the number of parallel turns increase, eddy current losses due to the PM field decreases dramatically due to reduction in the wire diameter. Therefore, the designs with a high number of parallel turns have lower copper losses, as can be seen from the results.

In total, nine non-dominated designs (the designs with the same number of parallel turns are compared) are chosen according to the Pareto-front approach for n= 1, 2, 4, and 6. Odd parallel turn numbers are not chosen due to their more complicated winding geometries. The selected designs are labelled on the Figure 6 and their attributions are given in Table 2. These designs are compared in terms of their costs, weights, and efficiencies in Section 3.2. Before these comparisons, analytical calculations used in the design process are validated using the FEA results.

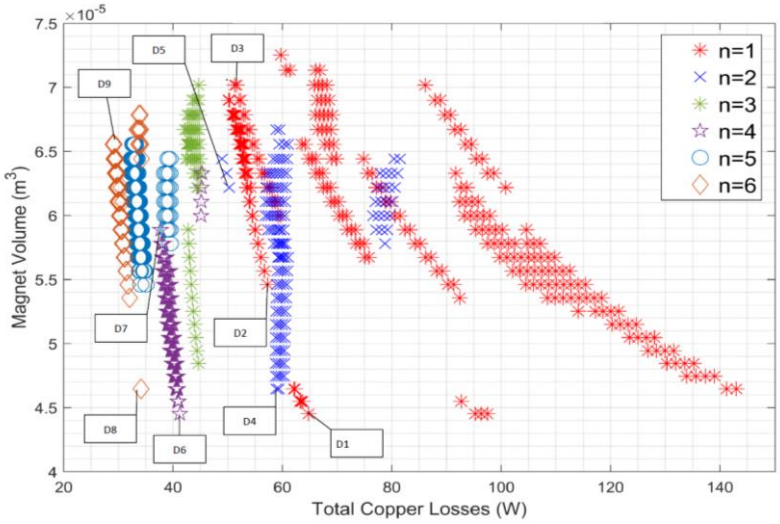

Figure 6. Designs with different number of paralel turns n shown as a function of their magnet volume and total copper loss that includes open-circuit winding losses.

Table 2. General attributions of non-dominated chosen designs.

	D1	D2	D3	D4	D5	D6	D7	D8	D9
Magnet radius (mm)	11.4	12.4	13.8	12.5	13.3	11.4	12.8	11.6	13.4
Inner yoke radius (mm)	17.4	17.5	18.1	18.4	18.3	17.4	18.8	17.3	18.9
Air-gap (mm)	6	5.1	4.3	5.9	5	6	6	5.7	5.5
Magnet volume (cm^3)	44.5	54.6	70.2	46.5	64.4	44.5	58.8	46.5	65.6
Stator volume (cm^3)	136	135	126	121	123	136	115	138	113
Series turn number	10	9	8	10	9	10	10	10	9
Parallel turn number	1	1	1	2	2	4	4	6	6
Wire diameter (mm)	1.15	1.15	0.91	1.15	1.02	0.81	0.81	0.64	0.64
Lstraight (mm)	10	10.3	11	11.5	10.9	10	10.9	10	11.2
Area factor	0.93	0.92	0.92	0.92	0.92	0.93	0.92	0.93	0.92
Induced voltage (V)	30.3	26.6	29.3	33.8	29.8	30.3	35.3	30.8	29.2
Resistance (mΩ)	44	39.7	56	20.8	25	22	22.6	23.5	21.1
Inductance (μH)	15.7	13.1	10.5	7.8	6.3	3.9	3.9	2.7	2.1
Phase current (Apeak)	26.6	24.3	22.1	23.2	21.7	26.6	22	25.3	22.1
Total copper loss (W)	64.8	57.3	51.6	58.9	49	41.2	37.7	34.1	29

3.2. Validation of analytical results FEA simulations

The analytical results are compared with two-dimensional (2-D) and three-dimensional (3-D) FEA simulation results performed by using Ansys/Maxwell before proceeding to the next step. Comparisons aim to show the validity of the analytical design process. Design D2 is selected for validation purpose. The FEA models of the selected design and the winding configuration of the 3-D model are shown in Figure 7. As shown in Figure 7a, D2 has a two layer winding with 9 series turns per layer and 1 parallel turn. In 3-D simulations, a stranded winding with 9 series turns is defined.

First of all, the air-gap flux density distribution results are validated. In Figure 8, 2-D FEA results for the flux density distribution only due to the PM flux in the middle of the PM outer and stator inner surfaces is compared with the analytical results. The good match between the results shows the validity of the expression given in (8).

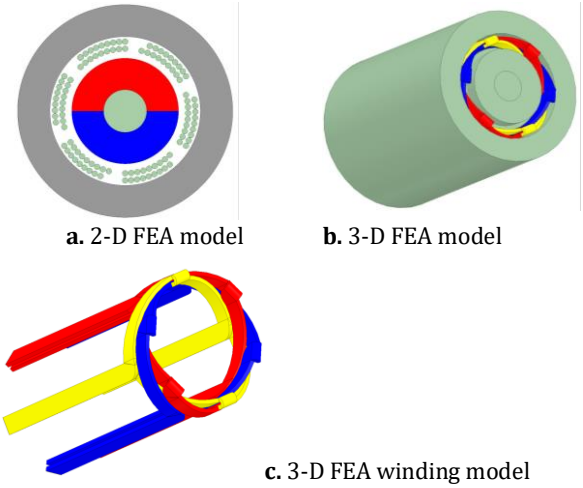

a. 2-D FEA model **b.** 3-D FEA model

c. 3-D FEA winding model

Figure 7. FEA models.

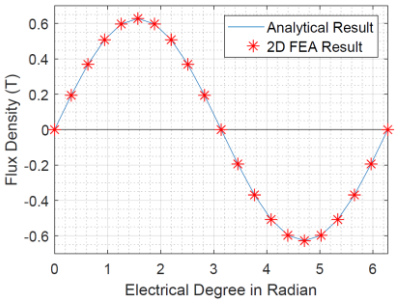

Figure 8. Flux density distribution in the air-gap.

Afterwards, the maximum field density restriction in the stator is examined. Field density distributions at no-load and rated-load operations are shown in Figure 9. It can be seen that the yoke flux densities do not exceed 1.7 T in both cases and there is no observable difference between the magnetic flux density distributions. This verifies the assumption made in the design process that the effect of the phase currents on the magnetic flux distribution is negligibly small. Slotless PM machines without winding overhangs have 3-D geometries and the output torque and induced voltage characteristics of such machines can only be simulated using 3-D models. Hence, first machine output characteristics comparisons are carried out between analytical and 3-D FEA results. Flux linkage induced back-EMF and torque output waveforms at rated conditions are shown in Figure 10.

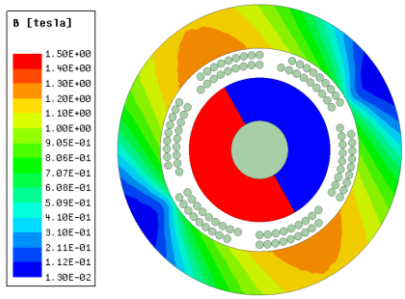

a. No load operation

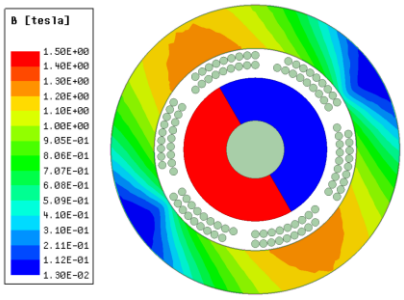

b. Rated-load operation

Figure 9. Flux density on the yoke.

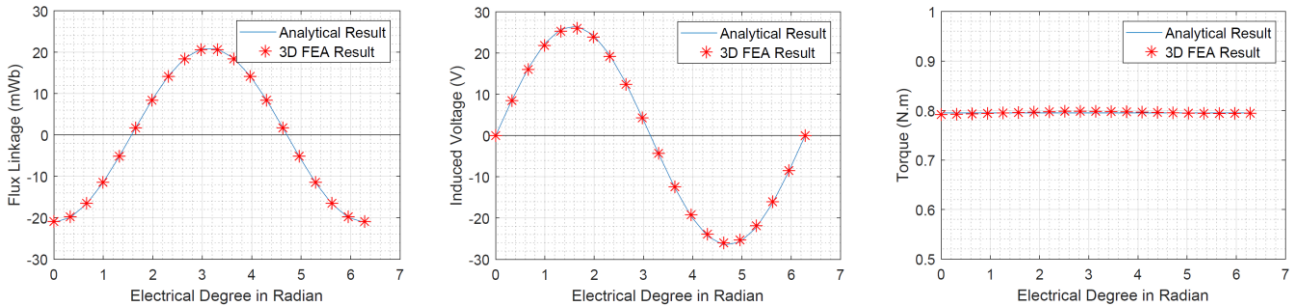

a. Flux Linkage **b.** Induced voltage **c.** Torque

Figure 10. Comparison of 3-D FEM model and analytical analysis results.

A very good match between the analytical and numerical results are observed. In Figure 10c, a very low torque ripple in numerical results is seen. Core magnetization and therefore the local relative permeability values change within the stator core material due to the non-linear material characteristics. This will create a small saliency that is dominantly due to the PM flux, which results in small variations in the torque output. This effect is considered in FEA model by using a non-linear B-H characteristic but ignored in the analytical calculations since the stator yoke is assumed to be infinitely permeable.

For torque calculation in FEA, a driver circuit is not used. Constant current and current angle are applied to the machine. These current and current angles are calculated by using analytical model. Torque output result which is obtained by FEA matches with analytical results.

Due to the higher computational cost of 3-D numerical analysis, 2-D analysis is adapted for this machine. In 2-D analysis, the machine is assumed to have the same cross-sectional structure throughout its axial length. Therefore, the correction factor that is used in the analytical calculations to account for the reduction in the winding area due to the hexagonal winding structure k_h is also applied to 2-D FEA model. To do that, the axial length of the machines are reduced by the multiplication factor k_h according to their dimensions. A similar correction factor is reported in 11. The correction factor should be used for flux linkage related computations but not for loss related calculations. The corrected 2-D FEA results are shown in Figure 11.

There is a less than 4% difference between the analytical and numeric results due to the assumption of a constant top angle α for all winding turns. This shows that 2-D FEA results can be used after correction factor is applied.

4. Discussion

To be able to identify the effects of the design decisions on machine performance, selected candidates are compared in terms of their costs, weights and efficiencies in Table 3. Costs of raw materials are taken as 78 $/kg for NdFeB magnets, 2.5 $/kg for electrical steel and 3 $/kg for copper. To ease comparisons, cost of D3 is taken as 100% and the relative costs of other designs are given in percentages. The designs with high amount of PM material are costlier than the designs with high amount of copper. For example, D3, D5, D7 and D9 have by far higher costs than that of D1, D4, D6 and D8.

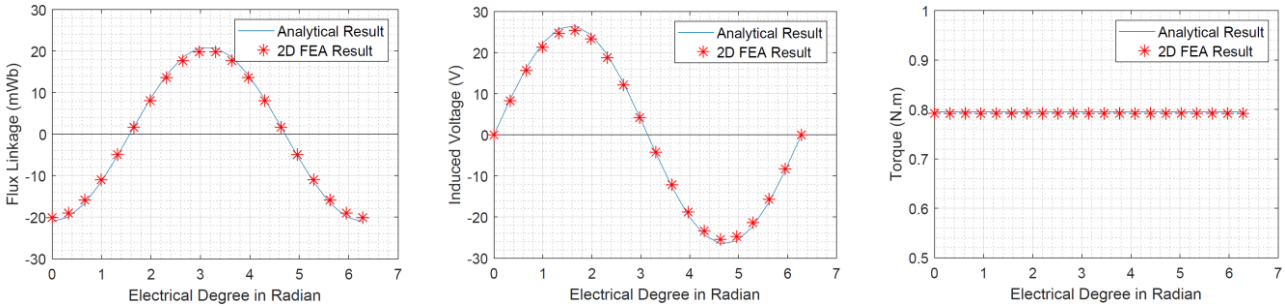

a. Flux Linkage **b.** Induced voltage **c.** Torque

Figure 11. Comparison of 2-D FEM model and analytical analysis results.

These results show one more time that PM volume minimization corresponds to cost minimization. The weight of the designs is very close to each other with a maximum difference of around 150g.

Further comparisons are carried out considering the losses and the efficiency at rated conditions. Two type of losses are considered: Total losses in the phase conductors and core loss in the stator. The PM and rotor core losses are ignored. It should be also mentioned that the mechanical losses are also not considered. The copper losses on the wires are known from the design process. As discussed earlier, copper losses tend to decrease as the number of parallel turns increase.

Moreover, core losses are obtained by using 2-D FEA simulations. Our design selection method was based on copper losses whereas core losses was assumed to be in the same range for all designs. This assumption is found to be partially valid. For example, D7 has the lowest copper losses and highest efficiency but D2 having the highest copper losses does not have the lowest efficiency. It must be mentioned here that the outer radius of the all designs is taken 25 mm, but some of designs could be produced with smaller outer dimensions by observing the flux density on their stator yoke, so their core losses may decrease. Moreover, copper losses are dominating in all designs as expected. This situation could be different for machines with higher pole-pair numbers and higher rotational speeds. By inspecting the cost and efficiency values, it can be concluded that some of the designs have superior characteristics. When the designs with one parallel turn that are D1, D2 and D3 are compared, it is seen that their efficiencies are approximately equal but D1 is cheaper. Thus, if manufacturability is considered for mass production, D1 is a strong candidate which is a good comprise between efficiency and ease of manufacturing. Furthermore, when all nine designs are compared, D6 can be identified as one of the designs with lowest cost and at the same time highest efficiency.

5. Conclusion

The presented slotless PM machine design approach is a powerful tool for comparison of the effects of various design decisions. The designs were created considering the manufacturability with conventional materials and techniques. Therefore, it can used by designers at the beginning of their design process for decision making. An optimized design was out of the scope of this study. However, the design approach can be combined with multi-objective optimization to find out the best design. The findings of this study will be very helpful to determine the objectives and constraints of the optimization. The objectives can be cost and efficiency for multi-objective optimization algorithms. As a future work, optimization of this motor will be constructed and optimal design will be obtained in terms of cost and efficiency.

This study contributed to the literature by showing the effects of the parallel turn number on machine efficiency. This effect will be much dominant at high speed applications. As a further study, the assessment of circulating currents between parallel turns of phase winding conductors can be suggested.

Ethics committee approval and conflict of interest statement

There is no need for an ethics committee approval in the current article. There is no conflict of interest with any person/institution in the current article.

Author contribution statement

Yusuf Basri Yilmaz: Conceptualization, investigation, methodology and software, visualization and writing – original draft. Emine Bostanci: Conceptualization, investigation, methodology, supervision and writing – review and editing.

References

[1] Min, S.G., Sarlioglu, B., 2018. Advantages and characteristic analysis of slotless rotary PM machines in comparison with conventional laminated design using statistical technique. IEEE Transactions on Transportation Electrification, Vol. 4(2), pp. 517–524. DOI: 10.1109/TTE.2018.2810230.

[2] Djelloul-Khedda, Z., Boughrara, K., Dubas, F., Kechroud, A., Souleyman, B., 2018. Semi-analytical magnetic field predicting in many structures of permanent-magnet synchronous machines considering the iron permeability. IEEE Transactions on Magnetics, Vol. 54(7). DOI: 10.1109/TMAG.2018.2824278.

[3] Zhu, Z.Q., Howe, D., Bolte, E., Ackermann, B., 1993. Instantaneous magnetic field distribution in brushless permanent magnet DC motors. IEEE Transactions on Magnetics, Vol. 29(1), pp. 124–135. DOI: 10.1109/20.195559.

[4] Xia, Z., Zhu, Z.Q., Howe, D., 2004. Analytical magnetic field analysis of Halbach magnetized permanent-magnet machines. IEEE Transactions on Magnetics, Vol. 40(4), pp. 1864–1872. DOI: 10.1109/TMAG.2004.828933.

[5] Rahideh, A., Korakianitis, T., 2012. Analytic magnetic field distribution of slotless brushless PM motors. Part 2: Open-circuit field and torque calculations. IET Electric Power Applications, Vol. 6(9), pp. 639–651. DOI: 10.1049/iet-epa.2011.0386.

[6] Tessarolo, A., Bortolozzi, M., Bruzzese, C., 2016. Explicit torque and back EMF expressions for slotless surface permanent magnet machines with different magnetization patterns. IEEE Transactions on Magnetics, Vol. 52(8), pp. 1–15. DOI: 10.1109/TMAG.2016.2543682.

[7] Chen, Y.S., Zhu, Z.Q., Howe, D., 1999. Slotless brushless permanent magnet machines: Influence of design parameters. IEEE Transactions on Energy Conversion, Vol. 14(3), pp. 686–691. DOI: 10.1109/60.790936.

[8] Marković, M., Perriard, Y., 2006. Simplified design methodology for a slotless brushless DC motor. IEEE Transactions on Magnetics, Vol. 42(12), pp. 3842–3846. DOI: 10.1109/TMAG.2006.884108.

[9] Pfister, J.P., Perriard, Y., 2010. Very-high-speed slotless permanent-magnet motors: Analytical modeling, optimization, design, and torque measurement methods. IEEE Transactions on Industrial Electronics, Vol. 57(1), pp. 296–303. DOI: 10.1109/TIE.2009.2027919.

[10] Kazerooni, K., Rahideh, A., Aghaei, J., 2016. Experimental optimal design of slotless brushless PM machines based on 2-D analytical model. IEEE Transactions on Magnetics, Vol. 52(5), pp. 1–16. DOI: 10.1109/TMAG.2016.2514505.
[11] Luomi, J., Zwyssig, C., Looser, A., Kolar, J.W., 2007. Efficiency optimization of a 100-W, 500 000-rpm permanent-magnet machine including air friction losses. In: 2007 IEEE Industry Applications Annual Meeting, 23–27 September, New Orleans, USA. DOI: 10.1109/07IAS.2007.135.
[12] Min, S.G., 2021. Modeling, investigation, and minimization of AC winding loss in slotless PM machines. IEEE Transactions on Energy Conversion, Vol. 36(3), pp. 2249–2260. DOI: 10.1109/TEC.2021.3050251.
[13] Seo, J.M., Kim, J.H., Jung, I.S., Jung, H.K., 2011. Design and analysis of slotless brushless DC motor. IEEE Transactions on Industry Applications, Vol. 47(2), pp. 730–735. DOI: 10.1109/TIA.2010.2091611.
[14] Burnand, G., Thabuis, A., Araujo, D.M., Perriard, Y., 2020. Novel optimized shape and topology for slotless windings in BLDC machines. IEEE Transactions on Industry Applications, Vol. 56(2), pp. 1275–1283. DOI: 10.1109/TIA.2019.2956717.
[15] Zhao, J., Wang, Y., Deng, L., Tang, L., Liu, X., He, W., 2023. Design and optimization of a slotless PMSM with hexagon distributed FPC winding. In: 2023 26th International Conference on Electrical Machines and Systems (ICEMS), China. DOI: 10.1109/ICEMS59686.2023.10344589.
[16] Lee, M., Koo, B., Nam, K., 2021. Analytic optimization of the Halbach array slotless motor considering stator yoke saturation. IEEE Transactions on Magnetics, Vol. 57(2), pp. 1–6. DOI: 10.1109/TMAG.2020.3019353.
[17] Lee, D., Balachandran, T., Sirimanna, S., Salk, N., Yoon, A., Xiao, P., Macks, J., Yu, Y., Lin, S., Schuh, J., Powell, P., Haran, K.S., 2022. Detailed design and prototyping of a high power density slotless PMSM. IEEE Transactions on Industry Applications, Vol. 59(2), pp. 1719–1727. DOI: 10.1109/TIA.2022.3230379.
[18] Gallego, G.B., Rossini, L., Achtnich, T., Araujo, D.M., Perriard, Y., 2021. Efficiency optimization of slotless magnetic-bearing machines. IEEE Transactions on Industry Applications, Vol. 57(6), pp. 6833–6843. DOI: 10.1109/TIA.2021.3072614.
[19] Rahideh, A., Korakianitis, T., 2012. Analytic magnetic field distribution of slotless brushless PM motors. Part 1: Armature reaction field, inductance and rotor eddy current loss calculations. IET Electric Power Applications, Vol. 6(9), pp. 628–638. DOI: 10.1049/iet-epa.2011.0385.
[20] Müller, G., Vogt, K., Ponick, B., 2007. Berechnung elektrischer Maschinen. John Wiley & Sons, pp. 440–453. DOI: 10.1002/9783527625079.